

Many-body effects in twisted bilayer graphene at low twist angles

A.O. Sboychakov,^{1,2} A.V. Rozhkov,^{1,2,3,4} A.L. Rakhmanov,^{1,2,3,5} and Franco Nori^{1,6}

¹Theoretical Quantum Physics Laboratory, RIKEN, Wako-shi, Saitama, 351-0198, Japan

²Institute for Theoretical and Applied Electrodynamics,
Russian Academy of Sciences, Moscow, 125412 Russia

³Moscow Institute for Physics and Technology (State University), Dolgoprudnyi, 141700 Russia

⁴Skolkovo Institute of Science and Technology, Skolkovo Innovation Center 3, Moscow 143026, Russia

⁵Dukhov Research Institute of Automatics, Moscow, 127055 Russia

⁶Department of Physics, University of Michigan, Ann Arbor, MI 48109-1040, USA

(Dated: December 14, 2024)

We study the zero-temperature many-body properties of twisted bilayer graphene with a twist angle equal to the so-called ‘first magic angle’. The system low-energy single-electron spectrum consists of four (eight, if spin label is accounted) weakly-dispersing partially degenerate bands, each band accommodating one electron per Moiré cell per spin projection. This weak dispersion makes electrons susceptible to the effects of interactions. Introducing several excitonic order parameters with spin-density-wave-like structure, we demonstrate that (i) the band degeneracy is partially lifted by the interaction, and (ii) the details of the low-energy spectrum becomes doping-dependent. For example, at or near the undoped state, interactions separate the eight bands into two quartets (one quartet is almost filled, the other is almost empty), while for two electrons per Moiré cell, the quartets are pulled apart, being replaced by four doublets. Such sensitivity to doping allows us to reproduce qualitatively the behavior of the conductance observed recently in experiments [Cao et al., *Nature* **556**, 80 (2018)]. Near half-filling, the electronic spectrum loses hexagonal symmetry indicating the appearance of a many-body nematic state.

PACS numbers: 73.22.Pr, 73.21.Ac

Introduction.— The search for broken-symmetry phases in graphene bilayer systems remains an active research area [1]. Theorists have studied a variety of possibilities, such as antiferromagnetism [2–10] superconductivity [11–15], excitons [3, 16–18], as well as more exotic states [5, 19]. Unfortunately, experimentally, the broken symmetry phases are rare celebrities in graphene systems, except, perhaps, AB bilayer graphene, for which numerous experiments [20–25] provide evidence of low-temperature non-superconducting order. It appears, however, that the situation in this field has changed: in recent experiments [26, 27] both superconductivity and many-body insulating states were detected in doped samples of twisted bilayer graphene (TBLG) whose twist angles θ are close to the so-called ‘first magic angle’ $\theta_c \approx 1.1^\circ$. The dependence of the conductance σ , as a function of doping n , showed several pronounced minima: at $n = 0$ (undoped state), at $n = \pm n_s/2$, and at $n = \pm n_s$ (the doping level $n = n_s$ corresponds to four electrons per supercell). In some samples, additional minima were observed at $n = \pm 3n_s/4$ [28], and at $n = n_s/4$ [29]. The purpose of this paper is to offer a theoretical explanation to these remarkable findings.

Our reasoning relies on the peculiar band structure of TBLG at small twist angles: for $\theta \leq \theta_c$, the low-energy single-electron spectrum is dominated by four (eight, if spin degeneracy is accounted) bands with almost no dispersion [30], and the Fermi surface is present even at zero doping [31] (provided that the interaction effects are neglected). The single-electron density of states (DOS)

of these bands offers a simple explanation [26] for the conductance minima at $n = \pm n_s$. As for the minima in the interval $-n_s < n < n_s$, such single-body reasoning fails to explain them, and a many-body formalism is necessary. Indeed, the flatness and degeneracy of the low-energy bands make them particularly susceptible to the interaction effects. To account for the latter, we use a mean-field approach. A simple on-site spin-density wave (SDW) order parameter is sufficient to reproduce the minimum at $n = 0$: in energy space, such an order parameter splits the eight bands into two quartets, one quartet is almost filled, the other is almost empty, with drastically reduced DOS at the Fermi level. To explain the behavior of $\sigma(n)$ at other n 's, the quartets must be split further (into doublets and singlets), which requires more complex SDW order parameters. The resultant formalism captures qualitatively the dependence of σ versus doping reported in Ref. 26.

Geometry of twisted bilayer graphene.— To introduce notation, let us start with brief review of basic TBLG geometrical facts [1, 32, 33]. A graphene monolayer has a hexagonal crystal structure consisting of two triangular sublattices A and B . The coordinates of atoms in layer 1 are $\mathbf{r}_n^{1A} = \mathbf{r}_n^1 \equiv n\mathbf{a}_1 + m\mathbf{a}_2$ and $\mathbf{r}_n^{1B} = \mathbf{r}_n^1 + \boldsymbol{\delta}$, where $\mathbf{n} = (n, m)$ is an integer-valued vector, $\mathbf{a}_{1,2} = a(\sqrt{3}, \mp 1)/2$ are the primitive vectors ($a = 2.46 \text{ \AA}$), and $\boldsymbol{\delta} = a(1/\sqrt{3}, 0)$. Atoms in layer 2 are located at $\mathbf{r}_n^{2B} = \mathbf{r}_n^2 \equiv d\mathbf{e}_z + n\mathbf{a}'_1 + m\mathbf{a}'_2$ and $\mathbf{r}_n^{2A} = \mathbf{r}_n^2 - \boldsymbol{\delta}'$, where $\mathbf{a}'_{1,2}$ and $\boldsymbol{\delta}'$ are the vectors $\mathbf{a}_{1,2}$ and $\boldsymbol{\delta}$, rotated by an angle θ . The unit vector along the z -axis is \mathbf{e}_z , the interlayer dis-

tance is $d = 3.35 \text{ \AA}$. The limiting case $\theta = 0$ corresponds to the AB stacking. The superstructure exists if $\cos \theta = (3m_0^2 + 3m_0r + r^2/2)/(3m_0^2 + 3m_0r + r^2)$, where m_0 and r are co-prime positive integers. The number of graphene unit cells inside a supercell is $N_{\text{sc}} = (3m_0^2 + 3m_0r + r^2)/g$ per layer, where $g = 1$ if $r \neq 3n$, or $g = 3$ otherwise. The reciprocal lattice primitive vectors for the layer 1 (layer 2) are denoted by $\mathbf{b}_{1,2}$ ($\mathbf{b}'_{1,2}$). For layer 1 one has $\mathbf{b}_{1,2} = 2\pi(1/\sqrt{3}, \mp 1)/a$, while $\mathbf{b}'_{1,2}$ are connected to $\mathbf{b}_{1,2}$ by rotating on angle θ . Using the notation $\mathcal{G}_{1,2}$ for the primitive reciprocal vectors for the superlattice, the following identities may be proven: $\mathbf{b}'_1 = \mathbf{b}_1 + r(\mathcal{G}_1 + \mathcal{G}_2)$ and $\mathbf{b}'_2 = \mathbf{b}_2 - r\mathcal{G}_1$ if $r \neq 3n$, or $\mathbf{b}'_1 = \mathbf{b}_1 + r(\mathcal{G}_1 + 2\mathcal{G}_2)/3$ and $\mathbf{b}'_2 = \mathbf{b}_2 - r(2\mathcal{G}_1 + \mathcal{G}_2)/3$, otherwise. The Brillouin zone of the superlattice is hexagonal-shaped. It can be obtained by N_{sc} -times folding of the Brillouin zone of the layer 1 or 2. Two non-equivalent corners of the reduced Brillouin zone, \mathbf{K}_1 and \mathbf{K}_2 , can be expressed via vectors $\mathcal{G}_{1,2}$ as $\mathbf{K}_1 = (\mathcal{G}_1 + 2\mathcal{G}_2)/3$ and $\mathbf{K}_2 = (2\mathcal{G}_1 + \mathcal{G}_2)/3$.

Model Hamiltonian.— We investigate the tight-binding model for p_z electrons in the TBLG at small doping n . The Hamiltonian is $\hat{H} = \hat{H}_0 + \hat{H}_{\text{int}}$, where \hat{H}_{int} is the electron-electron interaction, and a single-electron term is

$$\hat{H}_0 = - \sum_{\substack{injm \\ ss'\sigma}} t(\mathbf{r}_{\mathbf{n}}^{is}; \mathbf{r}_{\mathbf{m}}^{js'}) \hat{d}_{\mathbf{n}is\sigma}^\dagger \hat{d}_{\mathbf{m}js'\sigma}. \quad (1)$$

In this expression $\hat{d}_{\mathbf{n}is\sigma}^\dagger$ ($\hat{d}_{\mathbf{n}is\sigma}$) are the creation (annihilation) operators of the electron with spin σ at the unit cell \mathbf{n} in the layer i ($= 1, 2$) in the sublattice s ($= A, B$). For intralayer hopping, only the nearest-neighbor term is included. Its amplitude is $t = 2.57 \text{ eV}$. The interlayer hoppings are parameterized as described in Refs. [34, 35], with the largest interlayer hopping amplitude being equal to $t_0 = 0.4 \text{ eV}$. Switching to the momentum representation, one can introduce new single-particle operators $\hat{d}_{\mathbf{p}\mathbf{G}is\sigma} = \mathcal{N}^{-1/2} \sum_{\mathbf{n}} e^{-i(\mathbf{p}+\mathbf{G})\mathbf{r}_{\mathbf{n}}^i} \hat{d}_{\mathbf{n}is\sigma}$. Here \mathcal{N} is the number of graphene unit cells in the sample in one layer, the momentum \mathbf{p} lies in the first Brillouin zone of the superlattice, while $\mathbf{G} = m_1\mathcal{G}_1 + m_2\mathcal{G}_2$ is the reciprocal vector of the superlattice lying in the first Brillouin zone of the i th layer. The number of such vectors \mathbf{G} is equal to N_{sc} for each graphene layer. Thus, \hat{H}_0 becomes

$$\hat{H}_0 = \sum_{\mathbf{p}\mathbf{G}_{1,2}} \sum_{ijss'\sigma} \tilde{t}_{ij}^{ss'}(\mathbf{p}+\mathbf{G}_1; \mathbf{G}_1-\mathbf{G}_2) \hat{d}_{\mathbf{p}\mathbf{G}_1is\sigma}^\dagger \hat{d}_{\mathbf{p}\mathbf{G}_2js'\sigma}, \quad (2)$$

where the hopping amplitudes in momentum space are

$$\tilde{t}_{ij}^{ss'}(\mathbf{k}; \mathbf{G}) = \frac{1}{N_{\text{sc}}} \sum'_{\mathbf{nm}} e^{-i\mathbf{k}(\mathbf{r}_{\mathbf{n}}^i - \mathbf{r}_{\mathbf{m}}^j)} e^{-i\mathbf{G}\mathbf{r}_{\mathbf{m}}^j} t(\mathbf{r}_{\mathbf{n}}^{is}; \mathbf{r}_{\mathbf{m}}^{js'}). \quad (3)$$

The summation symbol with prime $\sum'_{\mathbf{nm}}$ implies that \mathbf{m} runs over sites inside the zeroth supercell, while \mathbf{n} runs over all sites in the sample.

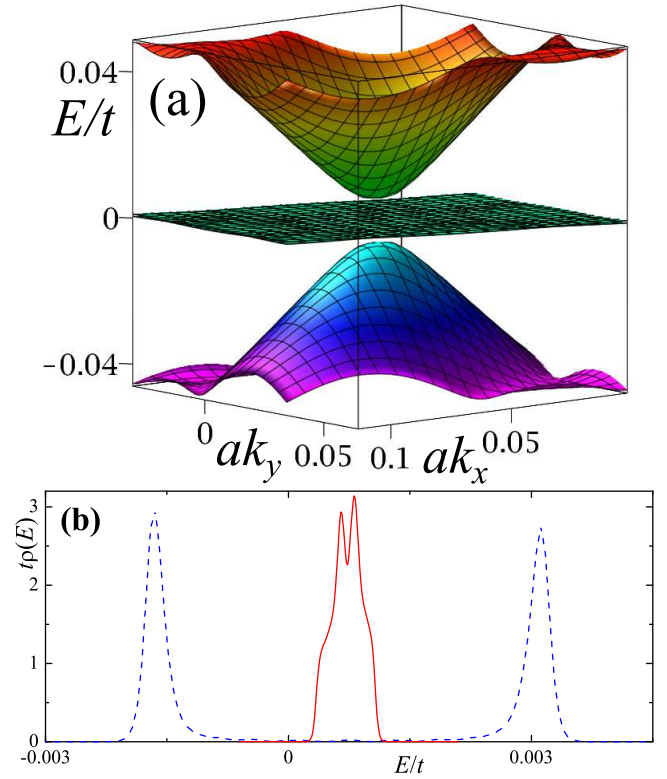


FIG. 1: (a) Single-particle low-energy band structure (interaction effects are neglected here) inside the superlattice Brillouin zone calculated for $\theta = \theta_c$. (b) Low-energy DOS $\rho(E)$ corresponding to the band structure shown above (solid curve) and for the band structure where interactions are taken into account (dashed curve), see Fig. 2(left) and text below.

Single-electron energies $E_{\mathbf{p}}^S$ and corresponding eigenvectors $\Phi_{\mathbf{p}\mathbf{G}is}^S$ (here $S = 1, 2, \dots, 4N_{\text{sc}}$ enumerates all $4N_{\text{sc}}$ bands of the TBLG) are found by numerical diagonalization of Eq. (2). The spectrum of (2) is well-studied. Its properties at small and large θ differ qualitatively. When $\theta > \theta_c$ (for the hopping parameters used here $\theta_c \approx 1.08^\circ$), the low-energy spectrum is Dirac-like. If $\theta \leq \theta_c$, the system acquires a Fermi surface, which is formed by four (eight, if spin degeneracy is accounted) almost-flat partially degenerate bands at low energy [30]. In Fig. 1 (a) the spectrum of this type is plotted for ‘the first magic angle’ $\theta = \theta_c$. We see that higher-energy electron and hole bands with pronounced dispersion are separated from each other by sheets of almost-flat bands. This peculiar spectrum structure is the origin of the many-body physics discussed below.

It is instructive to calculate the low-energy DOS $\rho(\varepsilon) = 2 \sum_S \int_{\mathbf{p}} \delta(E_{\mathbf{p}}^S - \varepsilon)$, see Fig. 1 (b). The DOS has a double peak structure, with the total spectral weight corresponding to eight electrons per a Moiré cell. The DOS remains non-zero for any doping in the interval $|n| < n_s$, as expected for a system with a Fermi surface [31]. The Fermi energy for the undoped state $n = 0$ corresponds

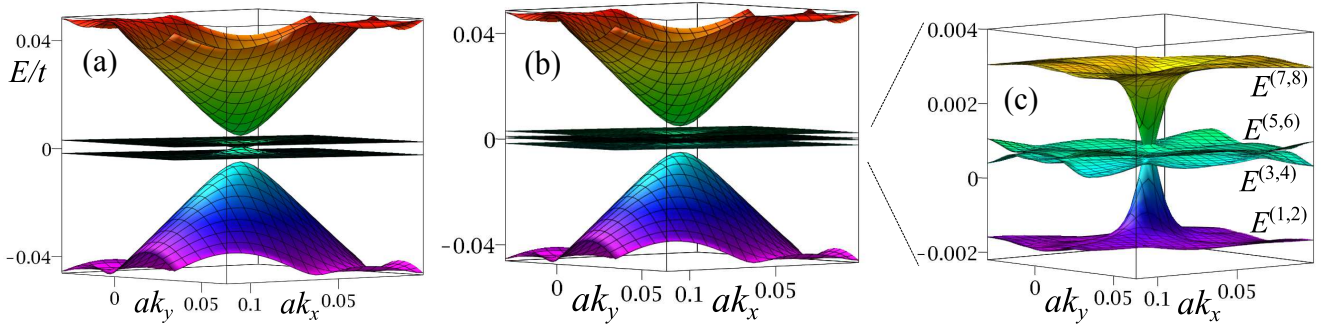


FIG. 2: (a) Low-energy band structure calculated self-consistently at $n = 0$. The eight bands are split into two quartets (individual bands are indiscernible due to small energy separations between them). (b) When $n = n_s/2$, the order parameter $A_{\mathbf{n}i\sigma}^{(\ell)}$ splits the two-quartet structure (left panel) into the doublet-quartet-doublet structure. (c) Fine structure of the low-energy bands for $n = n_s/2$. The energy bands are labeled by $E^{(\alpha)}$, $\alpha = 1 \dots 8$.

to the minimum on the DOS plot. The overall structure of the DOS plot and its width $W \sim 2$ meV are consistent with Fig. 1d of Ref. [27]. The flat bands are separated from the rest of the spectrum by two gaps, both of the order of 15 meV, in qualitative agreement with other computational [36] and experimental [27] results.

Interactions.— To model experimental conditions [26, 27], we study the many-body effects for $\theta = \theta_c$. As a starting point of our analysis, we model \hat{H}_{int} using the Hubbard interaction

$$\hat{H}_{\text{int}} = \frac{U}{2} \sum_{\mathbf{n}i\sigma} \hat{d}_{\mathbf{n}i\sigma}^\dagger \hat{d}_{\mathbf{n}i\sigma} \hat{d}_{\mathbf{n}i\bar{\sigma}}^\dagger \hat{d}_{\mathbf{n}i\bar{\sigma}}, \quad (4)$$

$$U = 2t < U_c^{\text{MF}}. \quad (5)$$

Here the notation $\bar{\sigma}$ means ‘not σ ’, and $U_c^{\text{MF}} \approx 2.23t$ is the critical strength for a single-layer graphene transition into a mean-field antiferromagnetic state [37]. The choice (5) implies that the interaction in our model is strong; yet, not strong enough to cause a single-layer many-body instability, at least in the mean-field framework. In other words, the presence of the second layer is a necessary prerequisite for a mean-field transition.

Two types of order parameters.— To account for the interaction (4) at the mean-field level, we must choose a suitable order parameter. First, let us define [3, 7, 8, 10, 38] the on-site magnetization $\eta_{\mathbf{m}i\sigma} = \langle \hat{d}_{\mathbf{m}i\sigma}^\dagger \hat{d}_{\mathbf{m}i\sigma} \rangle$, where $\langle \dots \rangle$ denotes the averaging with respect to the mean-field ground state. We will assume that the anomalous average $\eta_{\mathbf{m}i\sigma}$, as a function of position \mathbf{m} , has the same period as the superlattice. That is, only the spin-rotational symmetry is broken, while the superlattice translation symmetry is preserved (the spin texture has the same periodicity as the superlattice). Using the η ’s we decouple H_{int} , to obtain the mean-field interaction

$$\hat{H}_{\text{int}}^{\text{MF}} = \sum_{\mathbf{n}i\sigma} \left[-\Delta_{\mathbf{n}i\sigma} \hat{d}_{\mathbf{n}i\sigma}^\dagger \hat{d}_{\mathbf{n}i\sigma} + \frac{|\Delta_{\mathbf{n}i\sigma}|^2}{U} \right], \quad (6)$$

where $\Delta_{\mathbf{n}i\sigma} = U\eta_{\mathbf{n}i\sigma}$ is the order parameter. Find-

ing the self-consistent value of $\Delta_{\mathbf{n}i\sigma}$, we can determine the low-energy band structure of our model, modified by the interaction. Figure 2 (a) presents such calculations for $n = 0$. The order parameter $\Delta_{\mathbf{n}i\sigma}$ lifts the degeneracy of the low-energy spectrum, splitting the eight energy bands into two quartets: four bands are pushed above the Fermi level ε_F , and four other bands sink below ε_F . Each quartet appears as a peak in the DOS plot in Fig. 1(b). The peaks are separated by $E_g \approx 4.5 \times 10^{-3}t \approx 12$ meV. Although most of the electronic states are pushed away from the Fermi energy ε_F , near the Γ point the quartets cross the Fermi energy level, forming a Fermi surface, and generating a small but finite $\rho(\varepsilon_F)$. Thus, consistent with experiments [26], the undoped state is metallic. For further comparison, the (direction-averaged) charge conductance σ is evaluated in the τ -approximation

$$\sigma = \frac{e^2}{4\pi^2} \sum_S \int d^2\mathbf{p} \left| \partial E_{\mathbf{p}}^S / \partial \mathbf{p} \right|^2 \delta(\mu - E_{\mathbf{p}}^S) \tau(\mathbf{p}). \quad (7)$$

For calculations, a momentum-independent transport scattering time $\tau(\mathbf{p}) = \text{const.}$ is assumed. The dependence $\sigma = \sigma(n)$ demonstrates pronounced minimum at $n = 0$ [see Fig. 3(a)], which is also in agreement with data [26].

As for the conductance minima observed [26] near $n \approx n_s/2$ (near $n \approx -n_s/2$), we note that this doping level corresponds to two additional electrons (two additional holes) per supercell, or, equivalently, to complete filling (complete draining) of exactly two bands of the upper (lower) quartet. To generate an insulating state at this doping, a quartet must be split into two doublets, with the chemical potential lying between the doublets. Our mean-field calculations show that the order parameter (6) alone cannot do this, and an additional order parameter is required. To incorporate the latter into our theoretical framework, the interaction Hamiltonian, besides the Hubbard term (4), must have the term describing the (Coulomb) interaction of electrons on different

weaker feature at $n = n_s/4$. The available data suggests that (i) a conductance minimum emerges only when the value of doping is a multiple of $n_s/4$, (ii) *in a given sample*, not every value of n consistent with condition (i) necessarily hosts a minimum (the minima at $n \approx \pm 3n_s/4$ are present for D4, but are absent for D1; when $n \approx n_s/4$, only D1 demonstrates the minimum), and (iii) depending on sample, conductance at a given minimum may be metallic (all minima of D4 and the $n = 0$ minimum of D1), or insulating (D1 at $n = \pm n_s/2$). Our Fig. 3 (a) is consistent with (i): disregarding a weak minimum at $n \approx n_s/8$, all conductance minima can be associated with multiples of $n_s/4$. Our numerical calculations with a different model [41] for the interlayer hopping (to be presented elsewhere) show that minima at $\pm n_s/4$ and $\pm 3n_s/4$ are susceptible to delicate variations of microscopic details, and may disappear for some model parameters, in agreement with (ii). The value of the conductance at a given minimum demonstrates a similar sensitivity, which makes our proposal compatible with (iii).

Conclusions.— Using a mean-field approximation, we demonstrated that the low-energy flat bands of TBLG in the low- θ regime are very sensitive to interactions. Interactions destroy the partial degeneracy between these bands, inducing non-trivial many-body states, with magnetism and nematicity. The degeneracy is lifted in a different manner depending on the doping value. This microscopic feature is manifested macroscopically as a doping-controlled sequence of conductance minima, consistent with recent experimental observations [26].

This work is partially supported by the JSPS-Russian Foundation for Basic Research joint Project No. 19-52-50015. F.N. is supported in part by the MURI Center for Dynamic Magneto-Optics via the Air Force Office of Scientific Research (AFOSR) (FA9550-14-1-0040), Army Research Office (ARO) (Grant No. W911NF-18-1-0358), Asian Office of Aerospace Research and Development (AOARD) (Grant No. FA2386-18-1-4045), Japan Science and Technology Agency (JST) (the Q-LEAP, Impact program and CREST Grant No. JPMJCR1676), Japan Society for the Promotion of Science (JSPS) (JSPS-FWO Grant No. VS.059.18N), RIKEN-AIST Challenge Research Fund, and the John Templeton Foundation. A.V.R. is also grateful to the Skoltech NGP Program (Skoltech-MIT joint project) for additional support.

[1] A. Rozhkov, A. Sboychakov, A. Rakhmanov, and F. Nori, “Electronic properties of graphene-based bilayer systems,” *Phys. Rep.* **648**, 1 (2016).
 [2] M. Kharitonov, “Antiferromagnetic state in bilayer graphene,” *Phys. Rev. B* **86**, 195435 (2012).
 [3] R. S. Akzyanov, A. O. Sboychakov, A. V. Rozhkov, A. L. Rakhmanov, and F. Nori, “AA-stacked bilayer graphene in an applied electric field: Tunable antiferromagnetism

and coexisting exciton order parameter,” *Phys. Rev. B* **90**, 155415 (2014).
 [4] D. S. de la Peña, M. M. Scherer, and C. Honerkamp, “Electronic instabilities of the AA-honeycomb bilayer,” *Ann. Phys. (Leipzig)* **526**, 366 (2014).
 [5] Y. Lemonik, I. Aleiner, and V. I. Fal’ko, “Competing nematic, antiferromagnetic, and spin-flux orders in the ground state of bilayer graphene,” *Phys. Rev. B* **85**, 245451 (2012).
 [6] J. Nilsson, A. H. Castro Neto, N. M. R. Peres, and F. Guinea, “Electron-electron interactions and the phase diagram of a graphene bilayer,” *Phys. Rev. B* **73**, 214418 (2006).
 [7] A. O. Sboychakov, A. L. Rakhmanov, A. V. Rozhkov, and F. Nori, “Metal-insulator transition and phase separation in doped AA-stacked graphene bilayer,” *Phys. Rev. B* **87**, 121401 (2013).
 [8] A. O. Sboychakov, A. V. Rozhkov, A. L. Rakhmanov, and F. Nori, “Antiferromagnetic states and phase separation in doped AA-stacked graphene bilayers,” *Phys. Rev. B* **88**, 045409 (2013).
 [9] T. C. Lang, Z. Y. Meng, M. M. Scherer, S. Uebelacker, F. F. Assaad, A. Muramatsu, C. Honerkamp, and S. Wessel, “Antiferromagnetism in the Hubbard Model on the Bernal-Stacked Honeycomb Bilayer,” *Phys. Rev. Lett.* **109**, 126402 (2012).
 [10] A. L. Rakhmanov, A. V. Rozhkov, A. O. Sboychakov, and F. Nori, “Instabilities of the AA-Stacked Graphene Bilayer,” *Phys. Rev. Lett.* **109**, 206801 (2012).
 [11] J. L. McChesney, A. Bostwick, T. Ohta, T. Seyller, K. Horn, J. González, and E. Rotenberg, “Extended van Hove Singularity and Superconducting Instability in Doped Graphene,” *Phys. Rev. Lett.* **104**, 136803 (2010).
 [12] M. Y. Kagan, V. A. Mitskan, and M. M. Korovushkin, “Phase diagram of the Kohn-Luttinger superconducting state for bilayer graphene,” *EPJB* **88**, 157 (2015).
 [13] M. Y. Kagan, V. V. Val’kov, V. A. Mitskan, and M. M. Korovushkin, “The Kohn-Luttinger effect and anomalous pairing in new superconducting systems and graphene,” *JETP* **118**, 995 (2014).
 [14] J. González, F. Guinea, and M. A. H. Vozmediano, “Electron-electron interactions in graphene sheets,” *Phys. Rev. B* **63**, 134421 (2001).
 [15] Mohammad Alidoust, Morten Willatzen, and Antti-Pekka Jauho, “Symmetry of superconducting correlations in displaced bilayers of graphene,” *Phys. Rev. B* **99**, 155413 (2019).
 [16] Y. E. Lozovik and A. Sokolik, “Electron-hole pair condensation in a graphene bilayer,” *JETP Lett.* **87**, 55 (2008).
 [17] Y. E. Lozovik and A. Sokolik, “Multi-band pairing of ultrarelativistic electrons and holes in graphene bilayer,” *Phys. Lett. A* **374**, 326 (2009).
 [18] A. O. Sboychakov, A. V. Rozhkov, A. L. Rakhmanov, and F. Nori, “Externally Controlled Magnetism and Band Gap in Twisted Bilayer Graphene,” *Phys. Rev. Lett.* **120**, 266402 (2018).
 [19] F. Zhang and A. H. MacDonald, “Distinguishing Spontaneous Quantum Hall States in Bilayer Graphene,” *Phys. Rev. Lett.* **108**, 186804 (2012).
 [20] F. Freitag, M. Weiss, R. Maurand, J. Trbovic, and C. Schönberger, “Spin symmetry of the bilayer graphene ground state,” *Phys. Rev. B* **87**, 161402 (2013).
 [21] P. Maher, C. R. Dean, A. F. Young, T. Taniguchi,

- K. Watanabe, K. L. Shepard, J. Hone, and P. Kim, “Evidence for a spin phase transition at charge neutrality in bilayer graphene,” *Nat. Phys.* **9**, 154 (2013).
- [22] W. Bao, J. Velasco, F. Zhang, L. Jing, B. Standley, D. Smirnov, M. Bockrath, A. H. MacDonald, and C. N. Lau, “Evidence for a spontaneous gapped state in ultraclean bilayer graphene,” *PNAS* **109**, 10802 (2012).
- [23] H. J. van Elferen, A. Veligura, E. V. Kurganova, U. Zeitler, J. C. Maan, N. Tombros, I. J. Vera-Marun, and B. J. van Wees, “Field-induced quantum Hall ferromagnetism in suspended bilayer graphene,” *Phys. Rev. B* **85**, 115408 (2012).
- [24] F. Freitag, J. Trbovic, M. Weiss, and C. Schönerberger, “Spontaneously Gapped Ground State in Suspended Bilayer Graphene,” *Phys. Rev. Lett.* **108**, 076602 (2012).
- [25] J. Velasco Jr., L. Jing, W. Bao, Y. Lee, P. Kratz, V. Aji, M. Bockrath, C. Lau, C. Varma, R. Stillwell, et al., “Transport spectroscopy of symmetry-broken insulating states in bilayer graphene,” *Nat. Nano* **7**, 156 (2012).
- [26] Y. Cao, V. Fatemi, A. Demir, S. Fang, S. L. Tomarken, J. Y. Luo, J. D. Sanchez-Yamagishi, K. Watanabe, T. Taniguchi, E. Kaxiras, et al., “Correlated insulator behaviour at half-filling in magic-angle graphene superlattices,” *Nature* **556**, 80 (2018).
- [27] Y. Cao, V. Fatemi, S. Fang, K. Watanabe, T. Taniguchi, E. Kaxiras, and P. Jarillo-Herrero, “Unconventional superconductivity in magic-angle graphene superlattices,” *Nature* **556**, 43 (2018).
- [28] See Extended Data Figure 4 (b,c) in Ref. [26].
- [29] See Figure 2 (a) in Ref. [26].
- [30] Dirac cones [31, 32, 34, 42–44], which are used to approximate the low-energy spectrum for $\theta > \theta_c$, may persist even when $\theta < \theta_c$, yet, the Dirac-type dispersion may survive only in an extremely narrow energy range, of the order of a fraction of an meV; see, for example, Extended Data Figure 1 (g-l) in Ref. [26].
- [31] A. O. Sboychakov, A. L. Rakhmanov, A. V. Rozhkov, and F. Nori, “Electronic spectrum of twisted bilayer graphene,” *Phys. Rev. B* **92**, 075402 (2015).
- [32] J. M. B. Lopes dos Santos, N. M. R. Peres, and A. H. Castro Neto, “Continuum model of the twisted graphene bilayer,” *Phys. Rev. B* **86**, 155449 (2012).
- [33] E. J. Mele, “Interlayer coupling in rotationally faulted multilayer graphenes,” *J. Phys. D: Appl. Phys.* **45**, 154004 (2012).
- [34] G. Trambly de Laissardière, D. Mayou, and L. Magaud, “Numerical studies of confined states in rotated bilayers of graphene,” *Phys. Rev. B* **86**, 125413 (2012).
- [35] G. Trambly de Laissardière, D. Mayou, and L. Magaud, “Localization of Dirac Electrons in Rotated Graphene Bilayers,” *Nano Lett.* **10**, 804 (2010).
- [36] S. Carr, S. Fang, Z. Zhu, and E. Kaxiras, “Minimal model for low-energy electronic states of twisted bilayer graphene,” (2019).
- [37] S. Sorella and E. Tosatti, “Semi-Metal-Insulator Transition of the Hubbard Model in the Honeycomb Lattice,” *EPL (Europhysics Letters)* **19**, 699 (1992).
- [38] L. A. Gonzalez-Arraga, J. L. Lado, F. Guinea, and P. San-Jose, “Electrically Controllable Magnetism in Twisted Bilayer Graphene,” *Phys. Rev. Lett.* **119**, 107201 (2017).
- [39] In numerical procedure we take into account only bands inside the energy window $-0.25t < E_{\mathbf{p}}^S < 0.25t$. Contribution from higher-energy bands is taken into account effectively by introducing the term $-\sum_{\mathbf{nm}i\sigma} |\Delta_{\mathbf{nis}}|^2 / U_c - \sum_{\mathbf{nm}i\sigma} |A_{\mathbf{m}j\sigma}^{nis}|^2 / U_c$ with $U_c = 2.23t$.
- [40] A. Kerelsky, L. McGilly, D. M. Kennes, L. Xian, M. Yankowitz, S. Chen, K. Watanabe, T. Taniguchi, J. Hone, C. Dean, et al. (2018), arXiv:1812.08776.
- [41] M. S. Tang, C. Z. Wang, C. T. Chan, and K. M. Ho, “Environment-dependent tight-binding potential model,” *Phys. Rev. B* **53**, 979 (1996).
- [42] J. M. B. Lopes dos Santos, N. M. R. Peres, and A. H. Castro Neto, “Graphene Bilayer with a Twist: Electronic Structure,” *Phys. Rev. Lett.* **99**, 256802 (2007).
- [43] R. Bistritzer and A. H. MacDonald, “Moiré bands in twisted double-layer graphene,” *PNAS* **108**, 12233 (2011).
- [44] A. V. Rozhkov, A. O. Sboychakov, A. L. Rakhmanov, and F. Nori, “Single-electron gap in the spectrum of twisted bilayer graphene,” *Phys. Rev. B* **95**, 045119 (2017).